Structure-Dependent Electron Affinities of Perylene Diimide-based Acceptors

Ai Sugie[1], Weining Han[1], Nobutaka Shioya[2], Takashi Hasegawa[2], Hiroyuki Yoshida[1, 3*]

[1] Graduate School of Engineering, Chiba University, 1-33 Yayoicho, Inage-ku, Chiba, 263-8522, Japan
[2] Institute for Chemical Research, Kyoto University Uji, Kyoto, 611-0011, Japan
[3] Molecular Chirality Research Center, Chiba University, 1-33 Yayoicho, Inage-ku, Chiba, 263-8522, Japan

Abstract

Perylene dyes are a representative framework of electron transport (n-type) organic semiconductors. The energy of their electron transport level is electron affinity (EA), which is an important parameter in selecting the electron transport materials for device application and of the material's electron accepting ability. Recent studies show that EA may vary by as much as 1 eV depending on the molecular orientation owing to the electrostatic potential generated by the quadrupole moments. Because perylene dyes have a large quadrupole moment, it is essential to discuss EA with combining the molecular orientation in the sample film. In this work, we determine the EAs of perylene diimide derivatives in the solid phase using low-energy inverse photoelectron spectroscopy (LEIPS), which was developed by one of the authors. By changing the substrate and the alkyl-chain length, we systematically investigate the relationship between EA and molecular arrangement in the film to derive the general trend of EA of perylene dyes. The results show that most of the perylene dyes' EAs are range from 3.7 to 4.0 eV.

*corresponding author: hyoshida@chiba-u.jp

Introduction

Conventional inorganic semiconductors are often doped to give n- or p-type transport properties in electronic devices.[1] Conversely, organic semiconductors are normally used without doping. Although undoped organic semiconductors are intrinsic semiconductors,[2-3] organic semiconductors with electron affinity (EA) above 3.5 eV often show preferential electron transporting properties (n-type transport properties). Compared with the hole transport (p-type) materials, the variety of n-type organic materials is limited. Among them, rylene dyes are one of the most important building blocks.[4-5] As shown in Figure 1, 3,4,9,10-perylenetetracarboxylic dianhydride (PTCDA), 3,4,9,10-perylenetetracarboxylic diimide (PTCDI) and its derivatives are representative materials. They have been extensively studied as a working layer of n-type organic field effect transistors [6-11] and as acceptors of non-fullerene organic solar cells.[12-18] They are also known as pigment red 224 (PTCDA) and pigment violet 29 (PTCDI) and include pigment red 179 (PTCDI with R=CH_3) and perylene black 31 (PTCDI with R=$C_6H_5CH_2CH_2$), which show excellent chemical, thermal and photochemical stability and high absorbance of visible photons.

These rylene dyes have a rylene core (that is, naphthalene and perylene) with two strong electron deficient units, dicarboxylic anhydride or dicarboxylic diimide groups, attached on either end. Figure 1 shows the electrostatic potential distributions of PTCDA and PTCDI molecules. This acceptor-donor-acceptor (A-D-A) structure gives rise to a large permanent quadrupole moment along the molecular long axis. The quadrupole tensor components calculated at the B3LYP/6-311+G(d,2p) level are Q_x=32.6, Q_y=41.7 and Q_z=-74.3 Debye Å for PTCDA and Q_x=17.7, Q_y=17.6 and Q_z=-35.2 Debye Å for PTCDI.[19] Recent studies have revealed that the electrostatic potential generated by the molecular quadrupole moments affects the energy levels in the solid phase. For example, the molecules with large quadrupole moments show orientation [20-23] and molecular mixing [24-25] dependent energy levels. To discuss EA as the electron transport level in the films, it is crucial not only to determine EA in the solid phase but also to examine the relationship between EA and molecular orientation.

The EAs of organic materials are often deduced from the reduction potential measured using cyclic voltammetry. This method cannot account for the solid-state effect such as the molecular orientation dependence. The optical gap is also used to estimate EA from the ionization energy determined using ultraviolet photoelectron spectroscopy (UPS). The optical gap is, however, usually 0.5-1 eV smaller than the transport gap in organic semiconductors.[26-30] The best method to examine EA in the solid state is inverse photoelectron spectroscopy (IPES). In IPES, an electron is incident to the sample surface and by detecting the photon generated by the radiative transition to an unoccupied state, we examine the density of state of the unoccupied state. As an electron is left in the electron conduction level in the final state of this transition, EA is effectively determined as the onset energy with reference to the vacuum level. Although the previous IPES causes serious damage to the organic samples, the development of low-energy inverse photoelectron spectroscopy (LEIPS) by one of the authors solved

the problem by reducing the incident electron energy to below the damage threshold of the organic materials.[31-33] In our previous work, we have demonstrated the orientation dependence of both ionization energy and EA and quantified the electrostatic and electronic polarization energies.[34-35]

In this work, we investigated the EAs of PTCDI and its derivatives (R=H, CH_3, C_8H_{15} and $C_{13}H_{27}$; hereafter abbreviated as C0, C1, C8 and C13, respectively) films using LEIPS. The molecular orientations were controlled using different substrates on which molecules were vacuum deposited, such as highly oriented pyrolytic graphite (HOPG) and graphene for face-on orientation and a naturally oxidized silicon wafer (SiO_2) for end-on orientation. The molecular orientations were examined using grazing incidence X-ray diffraction (GIXD) and p-polarized multiple angle incidence resolution spectrometry (pMAIRS).[36-38] We further evaluate the general trend of EA orientation dependence based on the calculated electrostatic potential created by the molecular quadrupole moment. The aim of this work is to derive a general trend of EAs of perylene dyes in connection with their film structure.

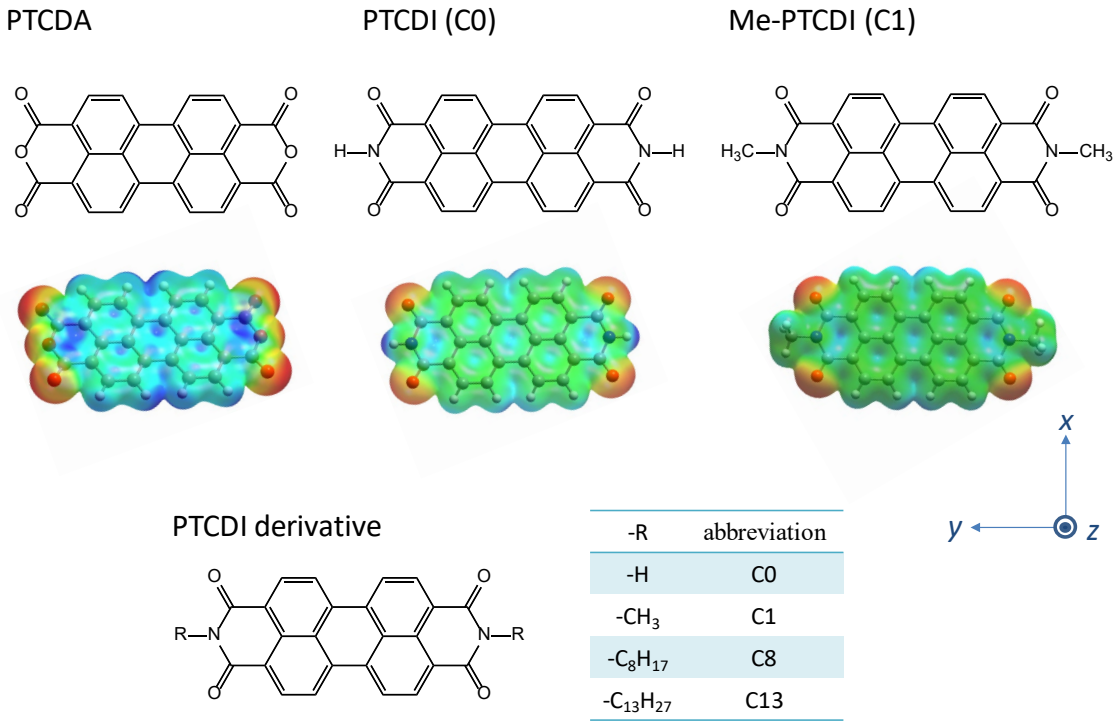

-R	abbreviation
-H	C0
$-CH_3$	C1
$-C_8H_{17}$	C8
$-C_{13}H_{27}$	C13

Figure 1: Molecular structures of rylene dyes and electrostatic potentials of PTCDA, PTCDI and Me-PTCDI. In the color maps, the red and blue surfaces correspond to the negative and positive potentials, respectively. The definition of molecular axes and abbreviations of PTCDI derivatives are also shown.

Experimental method

Materials were purchased from TCI Co. Ltd. and purified using vacuum sublimation. For the substrates, we used SiO_2, HOPG and graphene. SiO_2 was cleaned with acetone and isopropanol using an

ultrasonic cleaner and then annealed at 300 °C in vacuum (10^{-7} Pa in pressure). The graphene layer on SiO_2 (Graphene Platform) was heated at 150 °C for 30 min and then rinsed in acetone followed by annealing at 400 °C for 12 h in vacuum. HOPG was cleaved in air and annealed in vacuum for 400 °C for 10 h. The molecular material was deposited onto the substrate in vacuum (10^{-7} Pa in pressure) at a rate of 0.1-0.2 nm min^{-1}. The thickness and deposition rate were monitored using a quartz microbalance.

The prepared sample film was transferred to the LEIPS apparatus without exposing to air for in-situ measurement. The LEIPS apparatus is described elsewhere.[39] Briefly, electrons with kinetic energy between 0.0 and 5.5 eV are incident to the sample surface and the emitted photons are detected using a bandpass filter and photomultiplier tube. The center energy of the bandpass was 4.175 eV. The vacuum level was determined as the inflection point of the sample current measured as a function of electron energy.

The grazing incidence X-ray diffraction (GIXD) measurements were performed at BL46XU, SPring-8. The diffraction patterns were obtained by 2-dimensional X-ray detector (Pilatus 300K) in air with the incident angle of 0.12° of X-ray whose wavelength of 0.1 nm (12.39 keV in energy).

pMAIRS spectra were measured using a Thermo Fischer Scientific (Madison, WI, USA) Magna 550 FT-IR spectrometer equipped with Thermo Fisher Scientific (Yokohama, Japan) automatic MAIRS equipment (TN10–1500). The p-polarized IR light obtained by passing through a PIKE Technologies (Madison, WI, USA) manual polarizer (090–1500) was transmitted through the sample substrate with the angle of incidence changing from 9° to 44° in 5° steps. The transmitted light was detected using a mercury-cadmium-telluride detector. The detected signal was accumulated 500 times for each angle. Samples prepared on undoped silicon substrate were used for pMAIRS measurements.

Result

Molecular orientation

Figure 2 shows the GIXD patterns of the PTCDI films on the SiO_2 and graphene surfaces. To examine the molecular orientation from the GIXD data, we simulated the GIXD pattern based on the reported crystal structures according to a previously reported method.[40] The experimentally obtained patterns are well reproduced by the simulation based on the single crystal structures of C0,[41] C1,[42] C8,[43] and C13 [44] (Figure 2). The diffraction spots are indexed from the comparison between the experiment and the simulation.

In the diffraction pattern of C0/SiO_2, the diffraction of (020), ($11\bar{2}$) and ($12\bar{2}$) is observed normal to the substrate, which implies that the film contains crystallites with the three orientations. On the graphene surface, we observed the ($12\bar{2}$) reflection normal to the surface, which can be explained by only one crystallite orientation. In C1, we found large differences in the molecular orientation on

graphene and SiO_2. On graphene, we observed the (102) diffraction titled by 7° from the normal to the substrate where the C1 molecule has face-on orientation. On SiO_2, we observed the strong diffraction of (002) normal to the surface and a broad angular distribution (see also Figure S2), which indicates high mosaicity and suggests lower crystallinity than on the graphene. For C8, the diffraction patterns were similar between on graphene and SiO_2; the diffractions of (01L), L=1-5 were observed normal to the substrate likely because of the large cohesiveness ("fastener effect") owing to the long alkyl chains.[45-47] The diffraction pattern of C13/SiO_2 was similar to that of C8 and well reproduced by (001) orientation of the single crystal structure.[44] We did not observe clear diffraction from the C13/graphene.

From the orientations of the crystallite, the molecular orientations are determined as shown in Figure 2. C0 shows face-on orientation with the molecular long axis tilted by 80-90° from the surface normal for the films on the both substrates. The molecular long axis of C1 titled by 87.4° and 79.3° on graphene and broad distribution with a larger population from 77.6° to 90° on SiO_2. The PTCDI cores of the C8 and C13 molecules tilted by 50.6°.

The diffraction experiments examine only the crystalline part of the film because the ring shapes of the C0/SiO_2 and C1/SiO_2 diffractions suggest that the crystallinities of some of the films are not high and the films likely contain amorphous parts. To examine the average orientation of the whole molecules in the film, we performed pMAIRS measurement. The pMAIRS spectra determine the molecular orientation as the averaged direction of the transition dipole moment of each vibrational mode. We obtain the in-plane (IP) and out-of-plane (OP) IR spectra (Figure 3). The peaks are assigned by referring to the DFT calculation at the B3LYP/6-31G(d) level.[19] For C0 and C1, the band at ca. 1590 cm^{-1} is used for orientation analysis because the C=O stretching vibration (ν(C=O)) mode at 1697 cm^{-1} has a highly complicated shape. This band is assigned to the C–H in-plane deformation vibration (δ(C–H)) mode with a transition moment parallel to the long axis of the molecule. For C8 and C13, however, the δ(C–H) mode loses the character of the normal mode and enters a phone mode instead because the molecules are highly aggregated by the long alkyl chain. Therefore, the ν(C=O) mode is employed for orientation analysis. This mode also has the same direction as that of the long axis of the molecule. The orientation angle defined with respect to the substrate normal is calculated from the ratio of IP and OP intensities.[35-36]

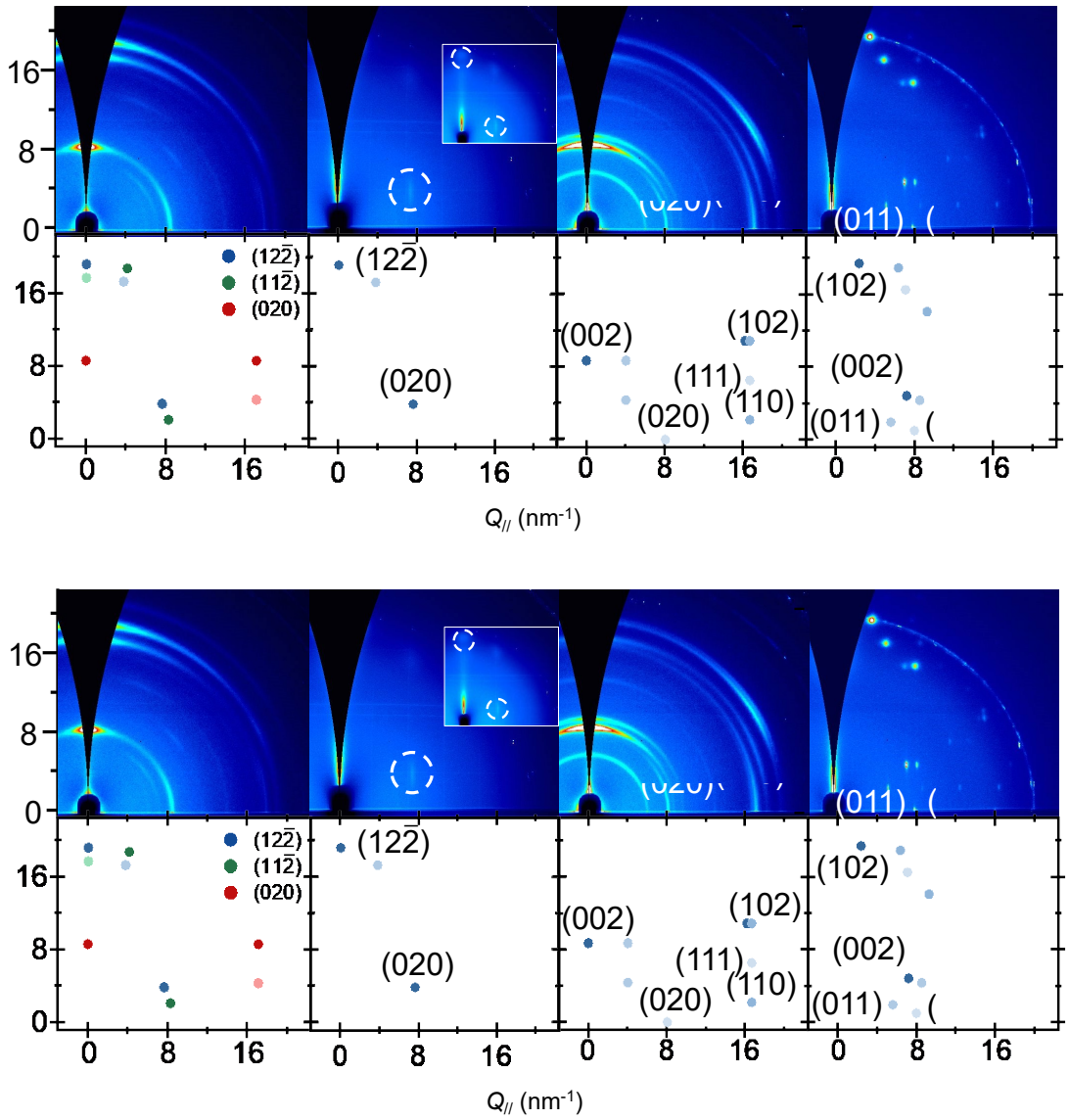

Figure 2: GIXD patterns of 10-nm-thick PTCDI-derivative films compared with the simulated diffraction pattterns based on the reported single crystal structures (see text). The diffraction intensity is shown versus the scattering vectors normal $Q_{\perp}$ and parallel $Q_{//}$ to the sample surface. In the inset of C0/graphene, an image without geometrical correction is presented so as to clearly show the $12\bar{2}$ reflection.

Table 1 summarizes the molecular orientations examined by GIXD and pMAIRS. The molecule without alkyl group C0 takes face-on orientation on both the SiO_2 and HOPG (or graphene) substrates. This is most likely due to the intralayer hydrogen bond. On the other hand, PTCDI with the long alkyl chains, C8 and C13, takes end-on orientation because the intermolecular fastener effect overcomes the

molecule-substrate interaction. This is generally observed that the molecules with longer alkyl chain preferentially grow with the end-on orientation. In PTCDI derivatives, R=C_4H_9 (C4) or longer may take the end-on orientation on any substrate.[48-49] The C1 molecule is an intermediate case that has face-on orientation on graphene (or HOPG) and a mixture of face-on and end-on orientations on SiO_2. It is interesting to note that the surfaces of C0 and C1 do not correlate with the molecular boundary in the crystal structures (Fig. S1). This may explain the large distributions of diffraction angles (large mosaicity) in the C0 and C1 films. On the contrary, the (001) surfaces correspond to the boundary of molecules showing small orientational distribution in C8 and C13 demonstrated by the sharp diffractions in GIXD.

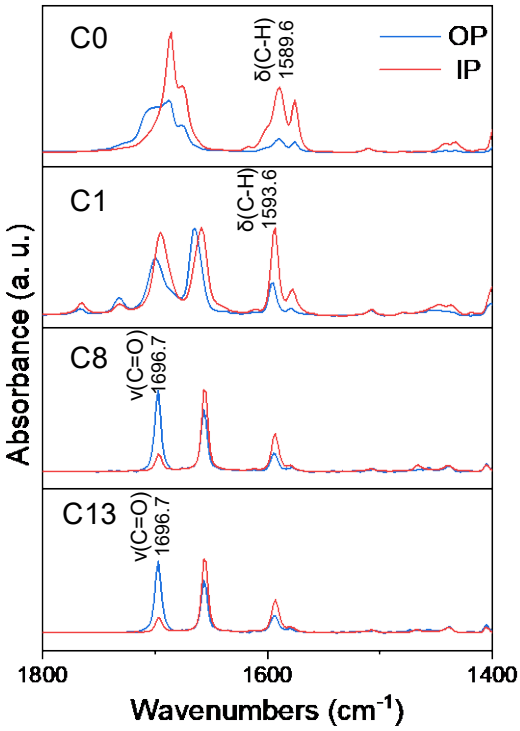

Figure 3: pMAIRS spectra of PTCDI-derivatives.

Table 1: Summary of molecular orientation and electron affinity (EA)

molecule	substrate	angle from normal to substrate (deg.)				electron affinity (eV)
		index	XRD		pMAIRS	
			molecule1	molecule2		
C0	SiO2	020	81.5	81.5	73.2	3.88
		11-2	88.6	84.5		
		12-2	89.3	82.9		
	graphene	12-2	89.3	82.9	-	3.95
C1	SiO2	002	77.6	77.6	67.1	4.12
	graphene	102	87.4	79.3	-	3.82
C8	SiO2, graphene	001	50.6	50.6	35.6	3.95
C13	SiO2	001	50.7	50.7	32.7	3.98

Electron affinities determined by LEIPS

Figure **4** shows thickness-dependent LEIPS spectra of the PTCDI-derivatives together with those of the bare substrates. This work aims to determine the EAs of materials with different molecular orientations without the effect of the substrate. Furthermore, molecules often take face-on orientation when the thickness is small and end-on or edge-on orientation when the thickness increases on HOPG or graphene. We examined the spectra as a function of film thickness up to 10 nm (5 nm for C1/SiO_2). As the thickness increases, the signal from the substrate disappears. For C0 and C1, the spectral feature is clearer in the film on HOPG. This is likely due to the higher structural order of the films on HOPG as discussed above. The intensities of C1 spectra depend on the molecular orientation. The first peak assignable to the LUMO of C1 is two times more intense on HOPG than SiO_2. The intensity of ultraviolet photoelectron spectroscopy spectrum is determined by the shape of molecular orbital (MO) and can be approximated by the Fourier transformation of the MO.[50-51] The same principle should be applied to the intensity of LEIPS because IPES is a time-inversion process of PES and the intensity is governed by Fermi's golden rule.[52] Therefore, the different intensities in the C1 spectra are due to the molecular orientations. Regarding C8 and C13, large differences were not observed except for the C13/HOPG. The reasons for the smaller intensity and absence of diffraction in GIXD of C13/HOPG are unclear. The film structure may be different or the sticking probability of C13 may be low on HOPG.

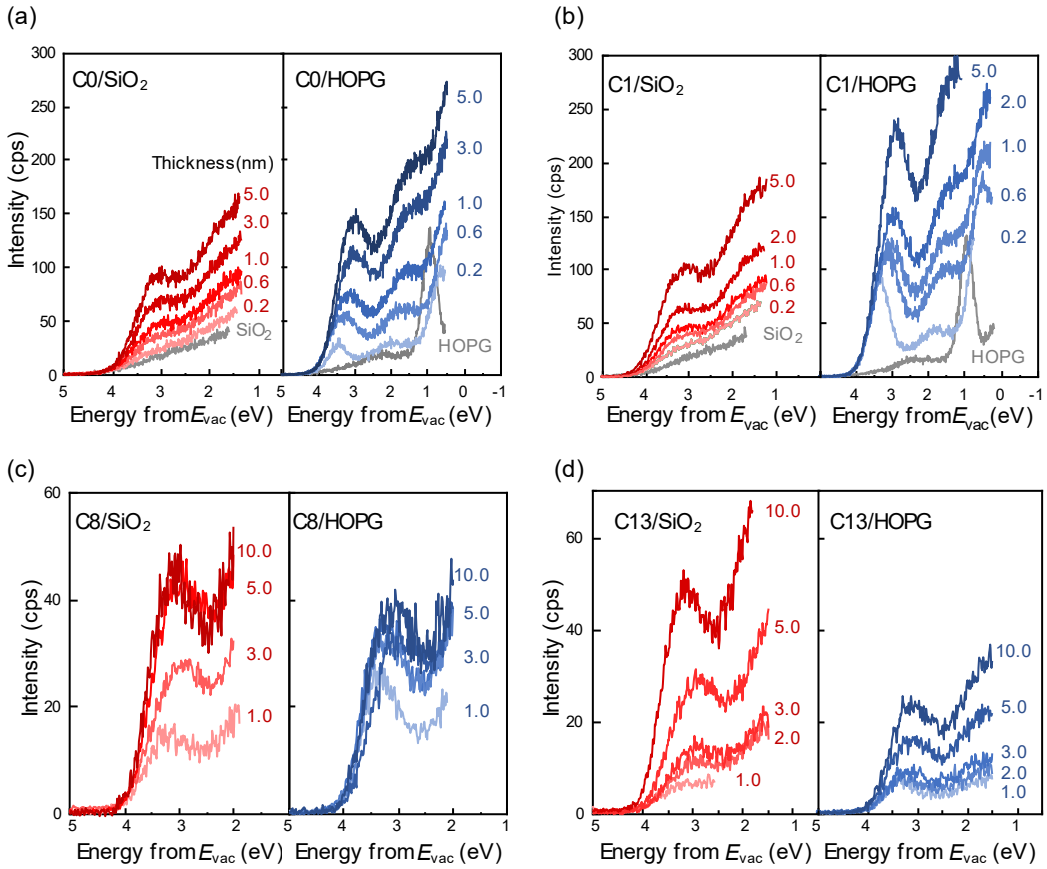

Figure 4: Thickness dependent LEIPS spectra of (a) C0, (b) C1, (c) C8 and (d) C13.

EA is determined as the onset energy of the LUMO derived peak (the first peak) with respect to the vacuum level. The values are shown in Figure 5. As the thickness reaches 5 nm, the EA no longer depends on film thickness. Thus, we determined the EA of the material at thicknesses of 5-10 nm. The EAs of C0 on SiO_2 and HOPG were 3.88 eV and 3.95 eV, respectively. The values are similar within the experimental uncertainties, which can be understood from the similar molecular orientations. The EAs of C8 and C13 were 3.92 eV and 3.98eV, respectively; these also do not depend on the substrates. The EAs are further examined through photon-energy dependent experiments for higher accuracy (Figures S4-S7). Conversely, the EAs of C1 on SiO_2 and HOPG differ by 0.3 eV at each thickness. The difference is described by the orientation dependent EA. From the EA at 5 nm thickness, we determined the EAs of C1 to be 4.16 eV on SiO_2 (close to end-on orientation) and 3.84 eV on HOPG (face-on). The EA values and molecular orientations are summarized in Table 1.

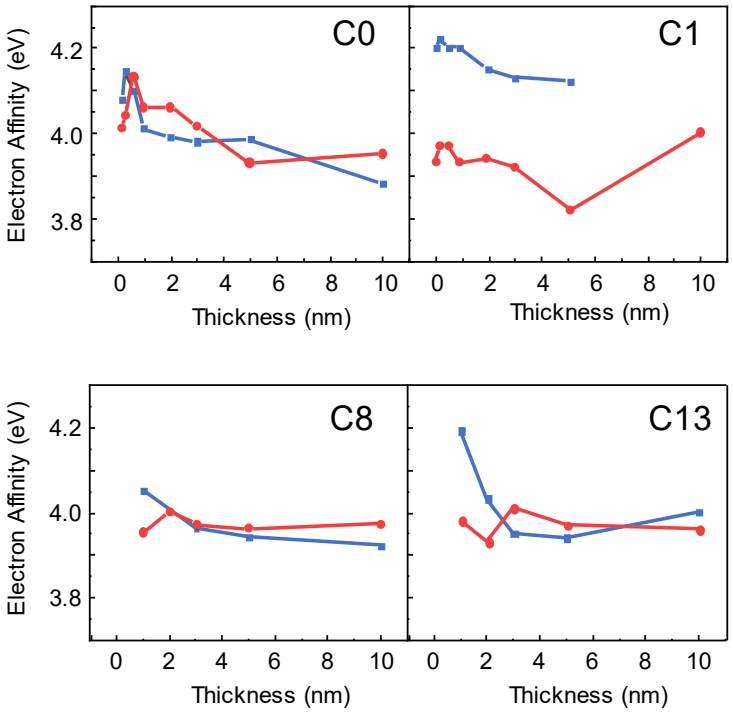

Figure 5: Electron affinities of PTCDI derivative films on SiO_2 (blue) and on HOPG (red) substrates as a function of film thickness.

Discussion

We have quantitatively examined the orientation dependent energy levels for highly ordered crystalline films such as pentacene [35] and pentacene-quinone.[34] The films of C0 and C1 contain crystallites with different orientations and an amorphous part. To further understand the relationship between molecular orientation and EA, we calculate the electrostatic potential generated by the molecular quadrupoles as we have done previously.[34] The calculation was performed for a disc-shaped cluster with radius r of 10 nm and the thicknesses d of 2, 4, 10 and 20 nm. A point quadrupole is distributed at the center of each molecule in the cluster. Potential maps of the cluster of C1 with r = 10 nm and d = 4 nm are shown in Figure S3. Because the results do not depend on the specific cluster size but only on the aspect ratio $d/2r$ of the disc, the electrostatic potential at the center of the cluster is shown as a function of $d/2r$ in Figure 6. As we have shown previously,[34] the electrostatic potential affects the energy levels when the aspect ratio is small and the electrostatic potential cancels out to show no orientation dependence as the aspect ratio approaches unity. Therefore, we can discuss the effect of electrostatic potential on the energy levels from the trend of the calculated energy as a function of aspect ratio.

In the C0 films, we observed in GIXD three crystal orientations – (020), $(11\bar{2})$ and $(12\bar{2})$ – on SiO_2

and only the $(12\bar{2})$ orientation on graphene. The calculated electrostatic potentials for the three crystal orientations in Figure 6 are quantitatively similar. The angles of the molecular long axes that are parallel to the quadrupole moments are similar, which explains the same EAs for C0 films on SiO_2 and HOPG (Figure 5). However, the LEIPS signal intensity depends on the substrate, which can be understood from the different orientation of the molecular planes. The (020) orientation is predominant in C0/SiO_2 and $(11\bar{2})$ in C0/HOPG; the molecular short axis and molecular plane orient differently (Figure S1). The observed EA of 3.9 eV for C0 can be compared with that of PTCDA. The PTCDA molecule also takes face-on orientation in the film because of the intermolecular hydrogen bond. The EA determined by LEIPS is 4.11 eV.[33] The slightly higher EA can be understood from the larger electron deficiency of dicarboxylic anhydride groups in PTCDA compared with the dicarboxylic diimide groups in C0 (PTCDI).

Regarding C1, the (002) axis is normal to the substrate and broadly distributed on SiO_2, whereas the (102) reflection shows a clear spot and a 7° tilt on HOPG. The calculated electrostatic potentials are similar, which disagrees with the observed EAs (Figure 5). Regarding the crystalline orientation distribution in the pole figure of C1/SiO_2 (Figure S2), the (002) axis was broadly distributed, which means that certain numbers of C1 molecules orient with the molecular long axis normal to the substrate. We calculated the electrostatic potential for films with the (002) axis parallel to the substrate (Figure 6b). This film has a higher EA owing to the end-on orientation of the constituent molecules (that is, the vertical orientation of the quadrupole moment), which is consistent with previous studies.[34-35]

We now consider the reason for the difference of about 0.3 eV in the observed EAs of C1 in terms of molecular orientation, though most molecules seem to show face-on orientation on both substrates. We examine the C1 films using three methods, GIXD, MAIRS and LEIPS. GIXD can observe the orientation of each crystallite separately but cannot detect the amorphous parts. MAIRS examines the average molecular orientation of both crystalline and amorphous parts. The spectral feature of LEIPS is the superposition of the features from all molecules in the film. The spectral line shape of the film on HOPG is shaper than that on SiO_2 (Figure 7a). This can be understood from the well-ordered structure of C1/HOPG supported by the sharp diffraction spots of C1/HOPG in GIXD. However, we determine EA from the onset of LEIPS spectra. The crystallite with the highest EA contributes to the onset region of the spectral feature; in the present case, the onset region of the LEIPS spectrum may reflect the EA of the molecules with end-on orientation.

To prove this hypothesis, we analyzed the spectral line shape of the LUMO peak of C1/SiO_2. Actual distribution of the crystalline in the film of C1/SiO_2 (Figure S2) is broad and intensity of the X-ray diffraction does not represent the real amount of the crystallite. We try to simulate the spectral line shape of C1/SiO_2 by superpositioning the spectra of different molecular orientation. We first assume that the C1/HOPG film contains homogeneously oriented molecules. Instead of assuming the continuous molecular orientation, we use three components, a C1/HOPG spectrum and those with the

energy shifted by 0.3 and 0.6 eV, because the observed difference in EA is 0.3 eV (Figure 7). We also assumed different numbers of components but arrived at the same conclusion. Consequently, we can conclude that the onset region of the observed peak in the C1/SiO_2 spectrum predominantly comprises end-on molecules and the peak region face-on molecules.

The calculated electrostatic potentials for C8 and C13 with (001) orientation show a subtle dependence of EA on the aspect ratio, which indicates little orientation dependence at the energy level. In this structure, the molecular long axis is titled by 50° according to GIXD and 35° by pMAIRS. We also calculated the electrostatic potential generated by the quadrupole moments that were vertically (0°) and horizontally (90°) distributed in the same lattice. The difference between the vertical and horizontal orientation decreases with as alkyl chain length increases (Figure 6). At an aspect ratio of 0.1, the difference is as much as 0.8 eV in C1 but only 0.4 eV in C8. To further examine the effect of the interlayer distance (the length of c^*-axis), we calculated the electrostatic potential of C8 with three orientations as a function of interlayer distance (Figure 8). When the interlayer distance decreases, the orientation dependence of energy levels indeed increases; for example, a two-fold increase when the interlayer distance is halved. This means that the molecular orientation dependence becomes less significant when (1) the molecular orientation is tilted or randomized from the vertical or horizontal orientation and (2) the interlayer distance is large.

In addition, the magnitude of molecular quadrupole moment decreases with the increase of the alkyl chain lengths. Figure S8 shows the calculated quadrupole moments.[19] The quadrupole tensor of acceptor-donor-acceptor (A-D-A) molecule has the maximum component along the A-D-A axis. The magnitude of quadrupole moment can be represented by the component along this axis, i.e. the maximum of the three components along the principal axes. By substituting oxygen in PTCDA with NH in PTCDI, the quadrupole moment is halved. From C0 to C1 or higher, it is reduced by a factor of 2/3. As depicted in the electrostatic potential of C1 (Figure 1), the methyl groups connected to the both end of the PTCDI core is positively charged which reduces the magnitude of the quadrupole moment. Thus, PTCDI derivative with long alkyl chains show the smaller orientation dependent energy levels because of the small quadrupole moment as well as the increased interlayer distance.

The above consideration strongly suggests that PTCDI derivatives with large substitute moieties show small orientation dependence. Further, EA is mostly determined by the PTCDI core and depends weakly on the alkyl groups, R. Calculated LUMO orbital energies by B3LYP/6-31G(d) (Figure S9)[19] clearly demonstrate that EA is almost independent of the alkyl chain length between C1 and C13 . This finding suggests that EA of PTCDI derivatives should be in the range between 3.7 and 4.0 eV. This is exemplified by EA of 3D-conjugated PTCDI derivatives.[53]

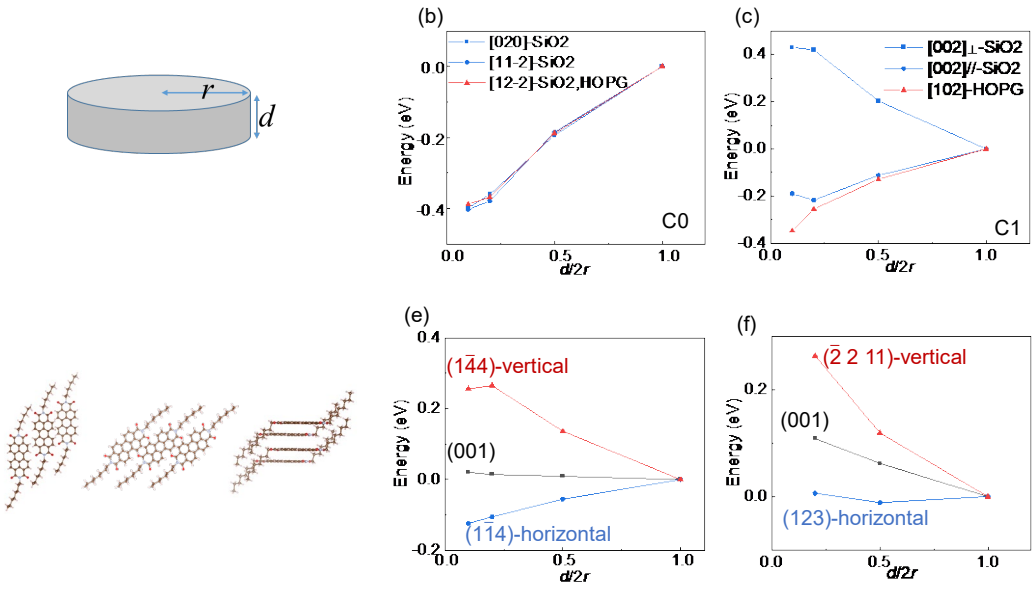

Figure 3: Electrostatic potential energies at the center of disk clusters as a function of aspect ratio *d/2r*. (a) Schematic of the cluster used for calculation of the polarization energies. Cluster of (b) C0 with 020, 11-2 and 12-2 orientations. (c) C1 with 002 and 102 orientations. (e) C8 and (f) C13 with 001, vertical and horizontal orientations. (d) molecular orientations of C8 used for calculation.

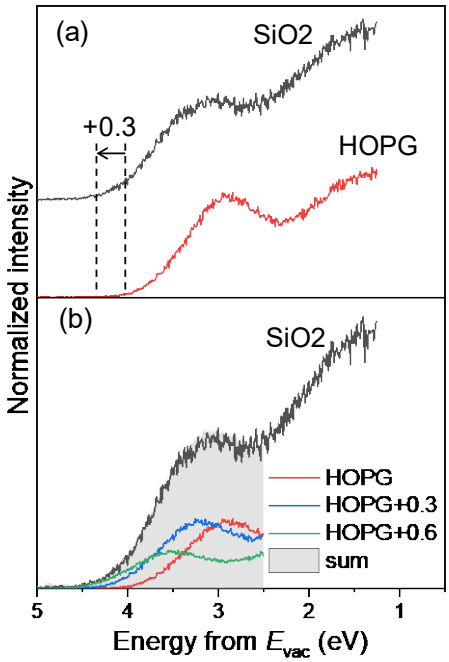

Figure 7: (a) LEIPS spectra of 5.0-nm-thick C1. (b) The shaded area shows the spectrum reproduced by the sum of three spectra on HOPG.

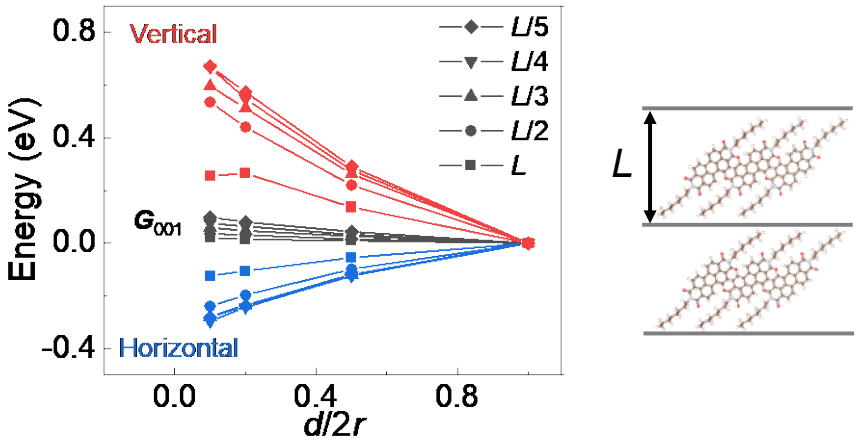

Figure 8: Distance dependent electrostatic potential energy of C8 and *L* defined as interlayer distance.

Conclusion

We discussed the EA of perylene dyes in the solid state using low-energy inverse photoelectron spectroscopy. Because the perylene dyes have large quadrupole moment along the molecular long axis, the large orientation dependence of EA is expected. We examined the relationship between EA and molecular orientation. We adopt PTCDI and its derivatives with linear alkyl chains to control the molecular orientation through alkyl chain length. The molecular orientations were examined using GIXD and pMAIRS, which can precisely examine the crystalline part and average molecular orientation of both crystalline and amorphous parts, respectively. GIXD patterns show that the films contain sometimes crystallites with different orientations or broad orientational distribution.

Non substituted PTCDI (C0) shows only face-on orientation because of intermolecular hydrogen bonds. The molecule substitute with methyl groups (C1) shows face-on orientation on HOPG (or graphene) and a mixture of face-on and end-on orientations on SiO_2. PTCDI with long alkyl chains (C8 and C13) shows end-on orientation because of the strong inter-chain interaction of the alkyl chains.

The observed EAs in face-on orientation are 3.9 eV and 3.8 eV for C0 and C1, respectively. These values are a little lower than the reported EA of 4.1 eV for PTCDA with face-on orientation because the imide of PTCDI has a weaker electron withdrawing nature than carboxylic anhydride of PTCDA. The results suggest that other PTCDI derivatives with face-on orientation have EAs of around 3.8 eV.

EAs of films with end-on orientation can be higher in small PTCDI derivatives because of the electrostatic potential generated by the vertically aligned quadrupole moments. The EA of the end-on C1 is 4.1 eV. The difference in EA between end-on and face-on orientations is 0.3 eV. However, PTCDI with longer alkyl chains gives smaller orientation dependence because of the prolonged interlayer distance and smaller molecular quadrupole moments. The electrostatic potentials are likely cancelled

out and EAs are 3.9 eV-4.0 eV in C8 and C13.

As for the recent non-fullerene acceptors for OSC, non-coplanarity is introduced to avoid aggregation.[54] Consequently, the direction of quadrupole moment is randomized. Further, long-alkyl chains are attached to the molecular cores to give good solubility. In this case, EA is not affected by electrostatic potential, as we have shown in this study. The EA value should be always about 3.7-4.0 eV if a big electron drawing unit (such as a halogen or cyano groups) is not introduced.

Supporting Information

The Supporting Information is available free of charge on the ACS Publications website at DOI:***. Molecular orientations determined by GIXD, diffraction intensity distribution of (002) reflection of C1/SiO_2, potential map of C1, LEIPS spectra measured at various photon energies, calculated quadrupole moments and HOMO/LUMO orbital energies of PTCDA and the perylene diimide molecules.

Acknowledgements

The 2D-GIXD measurements were performed at the BL46XU beamline of SPring-8 with the approval of the Japan Synchrotron Radiation Research Institute (JASRI). The authors thank Prof. Itaru Osaka of Hiroshima University and Dr. Tomoyuki Koganezawa for help with the GIXD experiments. This work was supported by the Advanced Low Carbon Technology Research and Development Program (ALCA) from Japan Science and Technology Agency (JPMJAL 1404), by KAKENHI from Japan Society for the Promotion of Science (26288007) and by the Futaba Foundation’s Futaba Research Grant Program.

ORCID

Takeshi Hasegawa 0000-0001-5574-9869

Hiroyuki Yoshida 0000-0002-8889-324X

References

1. Sze, S. M.; Ng, K. K., *Physics of Semiconductor Devices*: Wiley: **2006.**
2. Yasuda, T.; Goto, T.; Fujita, K.; Tsutsui, T., Ambipolar Pentacene Field-Effect Transistors with Calcium Source-Drain Electrodes. *Appl. Phys. Lett.* **2004,** *85*, 2098-2100.
3. Chua, L.-L.; Zaumseil, J.; Chang, J.-F.; Ou, E. C. W.; Ho, P. K. H.; Sirringhaus, H.; Friend, R. H., General Observation of N-Type Field-Effect Behaviour in Organic Semiconductors. *Nature* **2005,** *434,* 194-199.
4. Anthony, J. E.; Facchetti, A.; Heeney, M.; Marder, S. R.; Zhan, X., N-Type Organic Semiconductors in Organic Electronics. *Adv. Mater.* 2010, *22*, 3876-3892.
5. Zhan, X.; Facchetti, A.; Barlow, S.; Marks, T. J.; Ratner, M. A.; Wasielewski, M. R.; Marder, S. R., Rylene and Related Diimides for Organic Electronics. *Adv. Mater.* **2011,** *23,* 268-284.
6. Malenfant, P. R. L.; Dimitrakopoulos, C. D.; Gelorme, J. D.; Kosbar, L. L.; Graham, T. O.; Curioni, A.; Andreoni, W., N-Type Organic Thin-Film Transistor with High Field-Effect Mobility Based on a N,N'-Dialkyl-3,4,9,10-Perylene Tetracarboxylic Diimide Derivative. *Appl. Phys. Lett.* **2002,** *80,* 2517-2519.
7. Jones, B. A.; Ahrens, M. J.; Yoon, M.-H.; Facchetti, A.; Marks, T. J.; Wasielewski, M. R., High-Mobility Air-Stable N-Type Semiconductors with Processing Versatility: Dicyanoperylene-3,4:9,10-bis(dicarboximides). *Angew. Chem. Int. Ed*. **2004,** *43*, 6363-6366.
8. Ling, M.-M.; Erk, P.; Gomez, M.; Koenemann, M.; Locklin, J.; Bao, Z., Air-Stable N-Channel Organic Semiconductors Based on Perylene Diimide Derivatives without Strong Electron Withdrawing Groups. *Adv. Mater.* **2007,** *19*, 1123-1127.
9. Gsänger, M.; Oh, J. H.; Könemann, M.; Höffken, H. W.; Krause, A.-M.; Bao, Z.; Würthner, F., A Crystal-Engineered Hydrogen-Bonded Octachloroperylene Diimide with a Twisted Core: An N-Channel Organic Semiconductor. *Angew. Chem. Int. Ed*. **2010,** *49*, 740-743.
10. Würthner, F.; Stolte, M., Naphthalene and Perylene Diimides for Organic Transistors. *Chem. Commun.* **2011,** *47,* 5109-5115.
11. Zhao, Y.; Guo, Y. L.; Liu, Y. Q., 25th Anniversary Article: Recent Advances in N-Type and Ambipolar Organic Field-Effect Transistors. *Adv. Mater*. **2013,** *25*, 5372-5391.
12. Tang, C. W., Two‐Layer Organic Photovoltaic Cell. *Appl. Phys. Lett.* **1986,** *48,* 183-185.
13. Tang, C. W.; VanSlyke, S. A, Organic Electroluminescent Diodes. *Appl. Phys. Lett*. **1987,** *51*, 913-915.
14. Li, S.; Ye, L.; Zhao, W.; Zhang, S.; Mukherjee, S.; Ade, H.; Hou, J., Energy‐Level Modulation of Small‐Molecule Electron Acceptors to Achieve over 12% Efficiency in Polymer Solar Cells. *Adv. Mater.* **2016,** *28*, 9423-9429.
15. Zhao, D.; Wu, Q.; Cai, Z.; Zheng, T.; Chen, W.; Lu, J.; Yu, L., Electron Acceptors Based on A-

Substituted Perylene Diimide (PDI) for Organic Solar Cells. *Chem. Mater.* **2016,** *28,* 1139-1146.

16. Li, Z.; Yang, D.; Zhao, X.; Li, Z.; Zhang, T.; Wu, F.; Yang, X., New Pdi-Based Small-Molecule Cathode Interlayer Material with Strong Electron Extracting Ability for Polymer Solar Cells. *RSC Adv.* **2016,** *6,* 101645-101651.
17. Zhong, Y.; Trinh, M. T.; Chen, R.; Wang, W.; Khlyabich, P. P.; Kumar, B.; Xu, Q.; Nam, C.-Y.; Sfeir, M. Y.; Black, C., Efficient Organic Solar Cells with Helical Perylene Diimide Electron Acceptors. *J. Am. Chem. Soc.* **2014,** *136*, 15215-15221.
18. Li, C.; Wonneberger, H., Perylene Imides for Organic Photovoltaics: Yesterday, Today, and Tomorrow. *Adv. Mater.* **2012,** *24*, 613-636.
19. Frisch, M. J.; Trucks, G. W.; Schlegel, H. B.; Scuseria, G. E.; Robb, M. A.; Cheeseman, J. R.; Scalmani, G.; Barone, V.; Petersson, G. A.;Nakatsuji, H. et al., Gaussian 16, Revision B.01, Gaussian, Inc., Wallingford CT, 2016.
20. Duhm, S.; Heimel, G.; Salzmann, I.; Glowatzki, H.; Johnson, R. L.; Vollmer, A.; Rabe, J. P.; Koch, N., Orientation-Dependent Ionization Energies and Interface Dipoles in Ordered Molecular Assemblies. *Nat. Mater.* **2008,** *7*, 326-332.
21. Heimel, G.; Salzmann, I.; Duhm, S.; Koch, N., Design of Organic Semiconductors from Molecular Electrostatics. *Chem. Mater.* **2011,** *23*, 359-377.
22. Topham, B. J.; Soos, Z. G., Ionization in Organic Thin Films: Electrostatic Potential, Electronic Polarization, and Dopants in Pentacene Films. *Phys. Rev. B* **2011,** *84,* 165405.
23. Ryno, S. M.; Risko, C.; Bredas, J. L., Impact of Molecular Orientation and Packing Density on Electronic Polarization in the Bulk and at Surfaces of Organic Semiconductors. *ACS Appl. Mater. Interfaces* **2016,** *8,* 14053-14062.
24. Schwarze, M.; Tress, W.; Beyer, B.; Gao, F.; Scholz, R.; Poelking, C.; Ortstein, K.; Gunther, A. A.; Kasemann, D.; Andrienko, D.; Leo, K., Band Structure Engineering in Organic Semiconductors. *Science* **2016,** *352*, 1446-1449.
25. Schwarze, M.; Schellhammer, K. S.; Ortstein, K.; Benduhn, J.; Gaul, C.; Hinderhofer, A.; Perdigón Toro, L.; Scholz, R.; Kublitski, J.; Roland, S.; Lau, M.; Poelking, C.; Andrienko, D.; Cuniberti, G.; Schreiber, F.; Neher, D.; Vandewal, K.; Ortmann, F.; Leo, K., Impact of Molecular Quadrupole Moments on the Energy Levels at Organic Heterojunctions. *Nat. Commun.* **2019,** *10,* 2466.
26. Bredas, J. L.; Cornil, J.; Heeger, A. J., The Exciton Binding Energy in Luminescent Conjugated Polymers. *Adv. Mater.* **1996,** *8,* 447-452.
27. Knupfer, M.; Fink, J., Frenkel and Charge-Transfer Excitons in C_{60}. *Phys. Rev. B* **1999,** *60*, 10731-10734.
28. Knupfer, M., Exciton Binding Energies in Organic Semiconductors. *Appl. Phys. A* **2003,** *77*,

623-626.

29. Djurovich, P. I.; Mayo, E. I.; Forrest, S. R.; Thompson, M. E., Measurement of the Lowest Unoccupied Molecular Orbital Energies of Molecular Organic Semiconductors. *Org. Electron.* **2009,** *10,* 515-520.
30. Yoshida, H.; Yoshizaki, K., Electron Affinities of Organic Materials Used for Organic Light-Emitting Diodes: A Low-Energy Inverse Photoemission Study. *Org. Electron*. **2015,** *20*, 24-30.
31. Yoshida, H., Near-Ultraviolet Inverse Photoemission Spectroscopy Using Ultra-Low Energy Electrons. *Chem. Phys. Lett*. **2012,** *539-540,* 180-185.
32. Yoshida, H., Measuring the Electron Affinity of Organic Solids: An Indispensable New Tool for Organic Electronics. *Anal. Bioanal. Chem*. **2014,** *406,* 2231-2237.
33. Yoshida, H., Principle and Application of Low Energy Inverse Photoemission Spectroscopy: A New Method for Measuring Unoccupied States of Organic Semiconductors. *J. Electron Spectrosc. Relat. Phenom*. **2015,** *204,* 116-124.
34. Yamada, K.; Yanagisawa, S.; Koganezawa, T.; Mase, K.; Sato, N.; Yoshida, H., Impact of the Molecular Quadrupole Moment on Ionization Energy and Electron Affinity of Organic Thin Films: Experimental Determination of Electrostatic Potential and Electronic Polarization Energies. *Phys. Rev. B* **2018,** *97,* 245206.
35. Yoshida, H.; Yamada, K.; Tsutsumi, J.; Sato, N., Complete Description of Ionization Energy and Electron Affinity in Organic Solids: Determining Contributions from Electronic Polarization, Energy Band Dispersion, and Molecular Orientation. *Phys. Rev. B* **2015,** *92,* 075145.
36. Hasegawa, T., A Novel Measurement Technique of Pure Out-of-Plane Vibrational Modes in Thin Films on a Nonmetallic Material with No Polarizer. *J. Phys. Chem. B* **2002,** *106,* 4112-4115.
37. Hasegawa, T., Advanced Multiple-Angle Incidence Resolution Spectrometry for Thin-Layer Analysis on a Low-Refractive-Index Substrate. *Anal. Chem*. **2007,** *79*, 4385-4389.
38. Shioya, N.; Norimoto, S.; Izumi, N.; Hada, M.; Shimoaka, T.; Hasegawa, T., Optimal Experimental Condition of IR pMAIRS Calibrated by Using an Optically Isotropic Thin Film Exhibiting the Berreman Effect. *Appl. Spectrosc.* **2017,** *71,* 901-910.
39. Yoshida, H., Note: Low Energy Inverse Photoemission Spectroscopy Apparatus *Rev. Sci. Instrum*. **2014,** *85*, 016101.
40. Yoshida, H.; Inaba, K.; Sato, N., X-Ray Diffraction Reciprocal Space Mapping Study of the Thin Film Phase of Pentacene. *Appl. Phys. Lett.* **2007,** *90,* 181930.
41. Tojo, K.; Mizuguchi, J., Refinement of the Crystal Structure of 3,4:9,10-Perylenebis (Dicarboximide), $C_{24}H_{10}N_2O_4$, at 263 K. *Z. Kristallogr. NCS* **2002,** *217,* 45-46.
42. Hädicke, E.; Graser, F., Structures of Eleven Perylene-3,4:9,10-Bis(dicarboximide) Pigments. *Acta Crystallogr.* C **1986,** *42,* 189-195.
43. Briseno, A. L.; Mannsfeld, S. C.; Reese, C.; Hancock, J. M.; Xiong, Y.; Jenekhe, S. A.; Bao, Z.;

Xia, Y., Perylenediimide Nanowires and Their Use in Fabricating Field-Effect Transistors and Complementary Inverters. *Nano Lett.* **2007,** *7*, 2847-2853.

44. Tatemichi, S.; Ichikawa, M.; Koyama, T.; Taniguchi, Y., High Mobility N-Type Thin-Film Transistors Based on N, N'-Ditridecyl Perylene Diimide with Thermal Treatments. *Appl. Phys. Lett*. **2006,** *89*, 112108.
45. Inokuchi, H.; Saito, G.; Wu, P.; Seki, K.; Tang, T. B.; Mori, T.; Imaeda, K.; Enoki, T.; Higuchi, Y.; Inaka, K., A Novel Type of Organic Semiconductors. Molecular Fastener. *Chem. Lett.* **1986,** *15,* 1263-1266.
46. Kubozono, Y.; Hyodo, K.; Mori, H.; Hamao, S.; Goto, H.; Nishihara, Y., Transistor Application of New Picene-Type Molecules, 2,9-Dialkylated Phenanthro [1,2-b:8,7-b'] Dithiophenes. J. *Mater. Chem. C* **2015,** *3*, 2413-2421.
47. Kang, M. J.; Doi, I.; Mori, H.; Miyazaki, E.; Takimiya, K.; Ikeda, M.; Kuwabara, H., Alkylated Dinaphtho [2,3-b:2',3'-f] Thieno [3,2-b] Thiophenes (Cn‐DNTTs): Organic Semiconductors for High‐Performance Thin‐Film Transistors. *Adv. Mater.* **2011***, 23*, 1222-1225.
48. Alloway, D. M.; Armstrong, N. R., Organic Heterojunctions of Layered Perylene and Phthalocyanine Dyes: Characterization with UV-Photoelectron Spectroscopy and Luminescence Quenching. *Appl. Phys. A* **2009**, *95*, 209-218.
49. Arramel; Yin, X.; Wang, Q.; Zheng, Y. J.; Song, Z.; Bin Hassan, M. H.; Qi, D.; Wu, J.; Rusydi, A.; Wee, A. T. S., Molecular Alignment and Electronic Structure of N,N'-Dibutyl-3,4,9,10-Perylene-Tetracarboxylic- Diimide Molecules on Mos_2 Surfaces. *ACS Appl. Mater. Interfaces* **2017**, *9*, 5566-5573.
50. Kera, S.; Tanaka, S.; Yamane, H.; Yoshimura, D.; Okudaira, K. K.; Seki, K.; Ueno, N., Quantitative Analysis of Photoelectron Angular Distribution of Single-Domain Organic Monolayer Film: NTCDA on GeS(001). *Chem. Phys.* **2006,** *325,* 113-120.
51. Puschnig, P.; Berkebile, S.; Fleming, A. J.; Koller, G.; Emtsev, K.; Seyller, T.; Riley, J. D.; Ambrosch-Draxl, C.; Netzer, F. P.; Ramsey, M. G., Reconstruction of Molecular Orbital Densities from Photoemission Data. *Science* **2009,** *326*, 702-706.
52. Pendry, J. B., New Probe for Unoccupied Bands at Surfaces. *Phys. Rev. Lett*. **1980,** *45,* 1356-1358.
53. Ie, Y.; Karakawa, M.; Jinnai, S.; Yoshida, H.; Saeki, A.; Seki, S.; Yamamoto, S.; Ohkita, H.; Aso, Y., Electron-Donor Function of Methanofullerenes in Donor-Acceptor Bulk Heterojunction Systems. *Chem. Comm.* **2014**, *50*, 4123-4125.
54. Zhao, J.; Li, Y.; Lin, H.; Liu, Y.; Jiang, K.; Mu, C.; Ma, T.; Lin Lai, J. Y.; Hu, H.; Yu, D.; Yan, H., High-Efficiency Non-Fullerene Organic Solar Cells Enabled by a Difluorobenzothiadiazole-Based Donor Polymer Combined with a Properly Matched Small Molecule Acceptor. *Energy Environ. Sci.* **2015,** *8,* 520-525.

TOC graphic

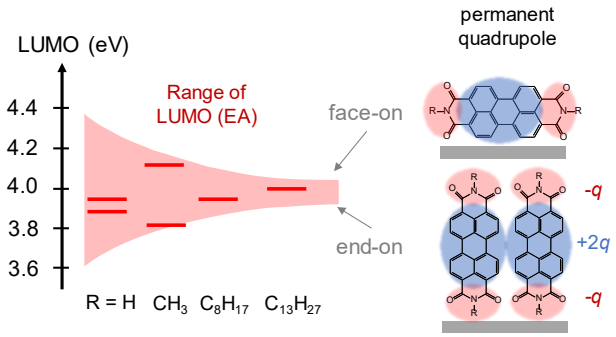
LUMO (eV)
4.4
4.2
4.0
3.8
3.6
Range of
LUMO (EA)
face-on
end-on
R = H CH3 C8H17 C13H27
permanent
quadrupole
-q
+2q
-q

Supporting Information

Structure-Dependent Electron Affinities of Perylene Diimide-based Acceptors

Ai Sugie[1], Weining Han[1], Nobutaka Shioya[2], Takashi Hasegawa[2], Hiroyuki Yoshida[1, 3*]

[1] Graduate School of Engineering, Chiba University,
1-33 Yayoicho, Inage-ku, Chiba, 263-8522, Japan

[2] Institute for Chemical Research, Kyoto University,
Uji, Kyoto, 611-0011, Japan

[3] Molecular Chirality Research Center, Chiba University,
1-33 Yayoicho, Inage-ku, Chiba, 263-8522, Japan

*Corresponding author: hyoshida@chiba-u.jp

Table of Contents

1. Molecular Orientations Determined by GIXD

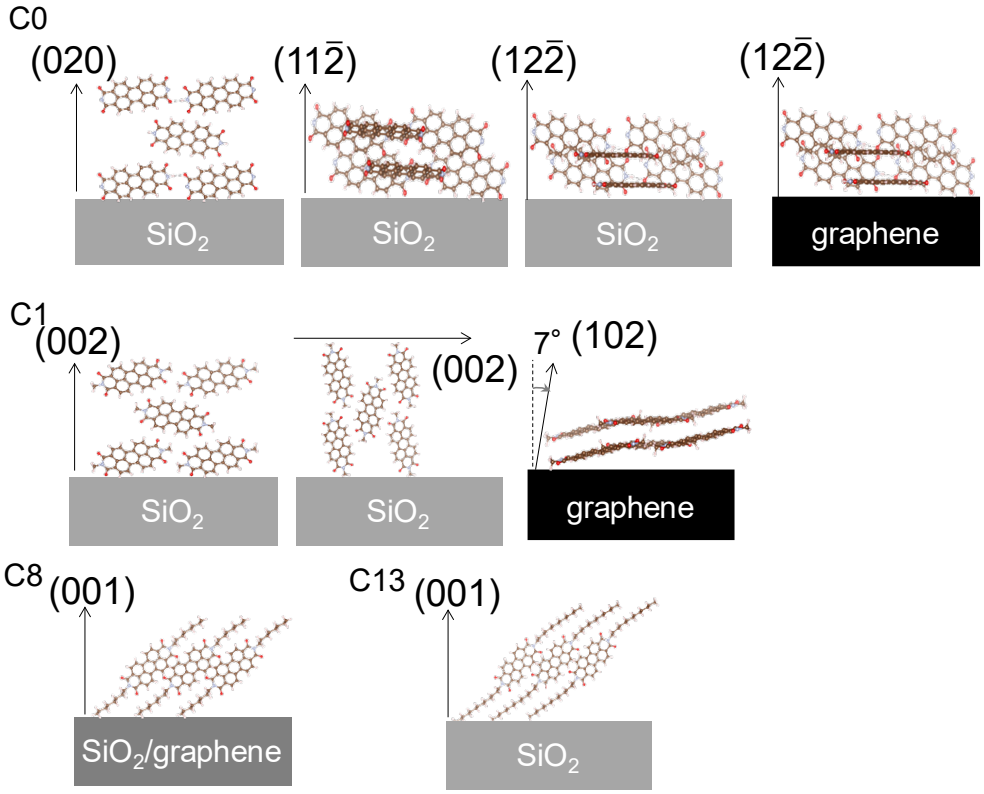

Figure S1: Molecular orienation deduced from the GIXD results.

2. Diffraction Intensity Distribution of (002) Reflection of C1/SiO_2

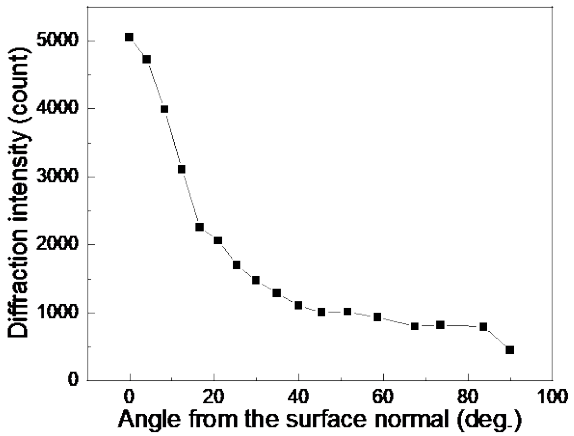

Figure S2: Intensity of (002) diffraction as a funciton of angle from the surface normal of C1/SiO_2 film showing the crystalline orientation distribution.

3.Potential Map of C1

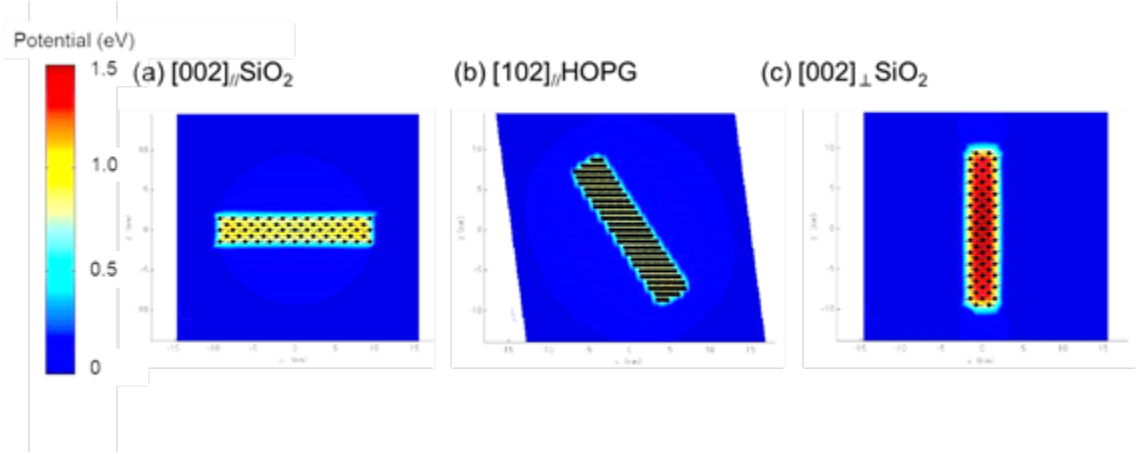

Figure S3: Potential maps of C1 for a disc-shape cluster with the radius r = 10 nm and the thickness d = 4 nm.

4. LEIPS Spectra Measured at Various Photon Energies

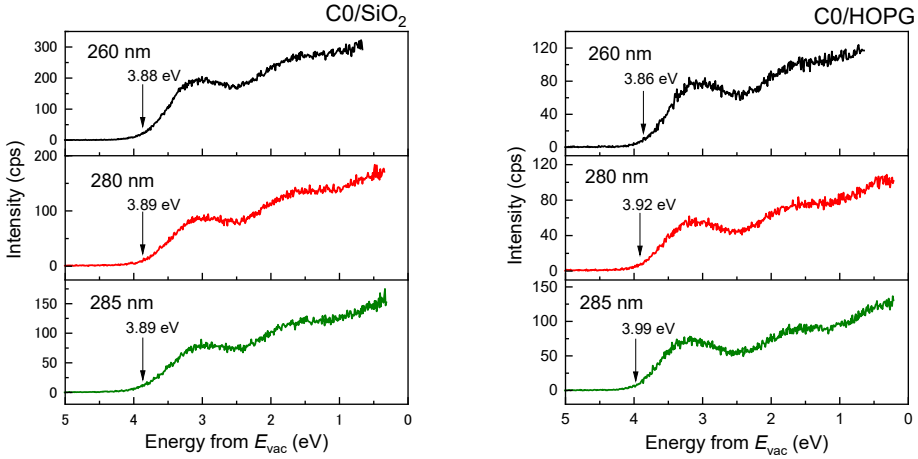

Figure S4: LEIPS spectra of 10 nm-thick C0 films taken at different wavelengths.

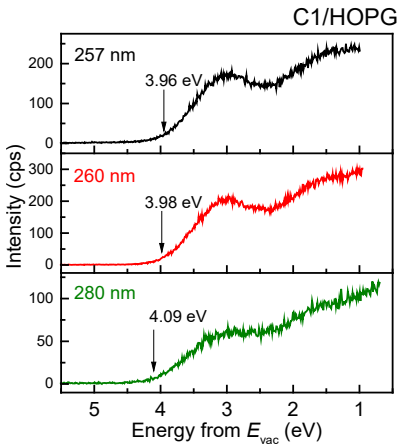

Figure S5: LEIPS spectra of 10 nm-thick C1 films taken at different wavelengths.

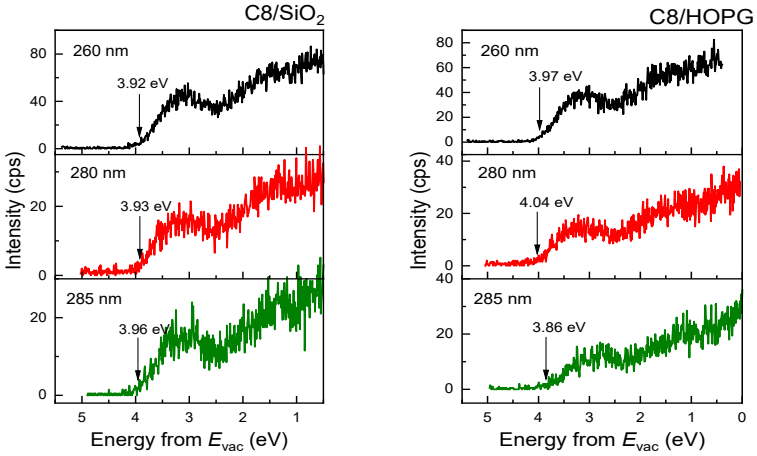

Figure S6: LEIPS spectra of 10 nm-thick C8 films taken at different wavelengths.

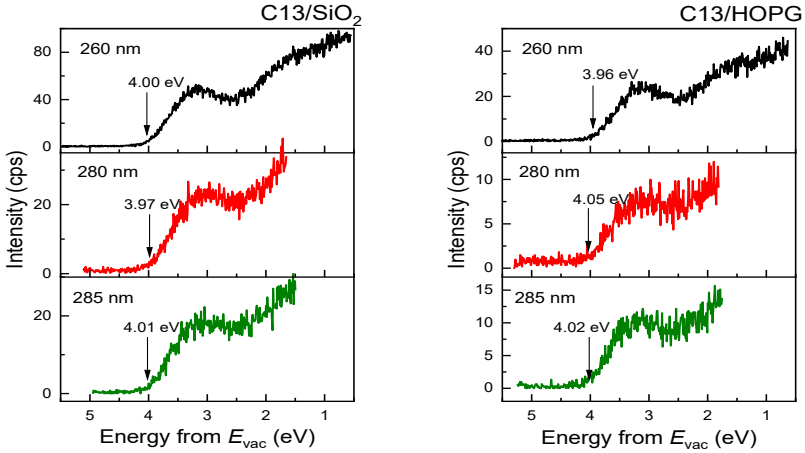

Figure S7: LEIPS spectra of 10 nm-thick C13 films taken at different wavelengths.

4. Calculated Quadrupole Tensors of PTCDA and Perylene Diimide molecules

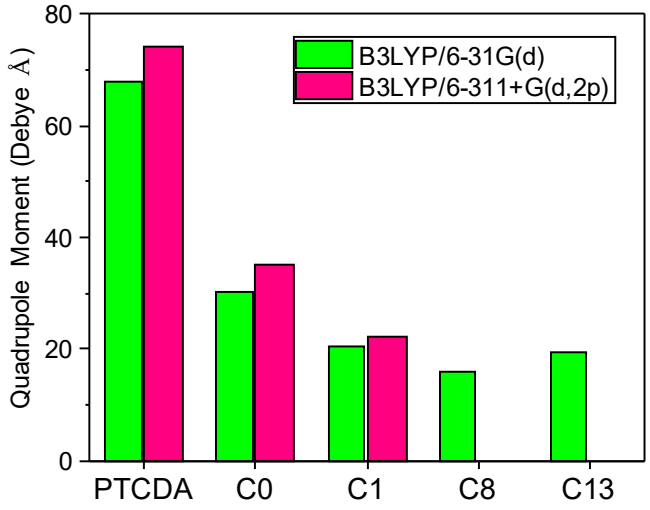

Figure S8: Quadrupole moments calculated at the theory of B3LYP/6-31G(d) and B3LYP/6-311+G(d,2p) levels. The maximum values along the principal axis are indicated (see text).

5. Calculated HOMO and LUMO Orbital Energies of PTCDA and Perylene Diimide Single Molecules

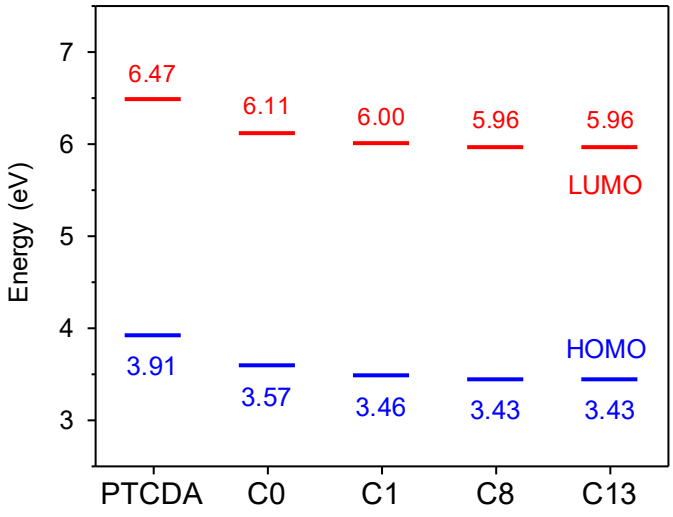

Figure S9: Calculated HOMO and LUMO levels at the theory of B3LYP/6-31G(d) level for single molecule (unit in eV). The HOMO and LUMO orbital energies are good measures of ionization energy and electron affinity of an isolated molecule, respectively.